Analysis on Chemical Reaction Kinetics of CuO/SiO2 Oxygen Carriers for Chemical Looping Air Separation

ARTICLE *in* ENERGY & FUELS · SEPTEMBER 2013

Impact Factor: 2.79 · DOI: 10.1021/ef401487x

5 AUTHORS, INCLUDING:

Hui Song
University of Newcastle
12 PUBLICATIONS **137** CITATIONS
SEE PROFILE

Kalpit Shah
University of Newcastle
39 PUBLICATIONS **225** CITATIONS
SEE PROFILE

Elham Doroodchi
University of Newcastle
77 PUBLICATIONS **472** CITATIONS
SEE PROFILE

T. F. Wall
University of Newcastle
191 PUBLICATIONS **5,261** CITATIONS
SEE PROFILE

energy&fuels

Article

pubs.acs.org/EF

Analysis on Chemical Reaction Kinetics of CuO/SiO_2 Oxygen Carriers for Chemical Looping Air Separation

Hui Song,[†] Kalpit Shah,[†] Elham Doroodchi,[‡] Terry Wall,[†] and Behdad Moghtaderi*[,†]

[†]Priority Research Centre for Energy, and [‡]Priority Research Centre for Advanced Particle Processing and Transport Chemical Engineering, School of Engineering, Faculty of Engineering and Built Environment, The University of Newcastle, Callaghan, New South Wales 2308, Australia

ABSTRACT: Chemical looping air separation (CLAS) offers an energy-efficient and cost-effective option for oxygen generation in several advanced power generation systems, such as integrated gasification combined cycle (IGCC), oxy-fuel combustion, and solid oxide fuel cells (SOFCs). In our previous study, CuO/SiO_2 has been identified as one of the most efficient oxygen carriers for the CLAS process because of its higher reactivity, greater oxygen transport capacity, and lower inventory requirement. In the current study, the kinetic analysis of CuO/SiO_2 oxygen carriers under a CLAS process environment has been conducted. The CuO/SiO_2 oxygen carriers with a varying CuO content of 18−48 wt % were prepared by a dry impregnation method. The redox behavior was investigated under N_2 and air separately for the temperature range of 800−975 °C in a thermogravimetric analyzer (TGA). The reduction rate was found to increase gradually with an increasing temperature, while in contrast, a drop in the oxidation rate was observed. Furthermore, the chemical reaction kinetics of 18 wt % CuO/SiO_2 for reduction and oxidation was attained by fitting various gas−solid reaction mechanisms with the obtained experimental data. Among all studied gas−solid reaction mechanisms, it was observed that the Avrami−Erofe'ev random nucleation and subsequence growth model (A2) and phase boundary reaction model (R2) fitted well with reduction and oxidation experimental data, respectively. In addition, relevant kinetic parameters, such as activation energy, pre-exponential factor, and reaction order, were also determined.

1. INTRODUCTION

Electricity generation from fossil fuels has been found to be responsible for roughly one-third of the global CO_2 emissions.[1−5] Although significant efforts have been made to replace fossil fuels by renewable energy resources, e.g., wind, solar, and nuclear power, because of their limited reliability and early state of the art development, they would not entirely replace the dominant use of fossil fuels in the several coming decades.[2] Under this scenario, one of the important measures to reduce the global CO_2 emissions in a relatively short time span is carbon capture and storage (CCS).[1−6] In the CCS route, oxy-fuel and integrated gasification and combustion of coal (IGCC) are a few among the several advanced clean coal technologies being developed with the potential of efficiently capturing CO_2. However, they may need large amount of oxygen rather than air, and thus, the viability of them is both technically and economically underpinned by the economic oxygen production.[7,8]

Oxygen is commonly produced at industrial scales through air separation using cryogenic distillation [cryogenic air separation unit (CASU)] and adsorption-based [pressure swing adsorption (PSA)/vacuum pressure swing adsorption (VPSA)] technologies.[7,9,10] Advanced technologies, such as membrane separation [e.g., ion-transport membrane (ITM)] and *in situ* air separation, are also being developed. The comparison of various oxygen production technologies are described elsewhere.[7,9,10] Despite being the most matured technology, CASU is highly energy-intensive. Approximately, 3−4% energy penalty is expected to arise for oxygen production using CASU for the oxy-fuel process.[7] As an alternative to CASU, the University of Newcastle, Australia, has invented and developed a new process called chemical looping air separation (CLAS), which is expected to offset 1−3% of the energy penalty associated with CASU.[7,8,10,11]

The working principle of the CLAS process is extremely simple and involves the cyclic oxidation (reaction 1) of metallic oxide particles by air and reduction (reaction 2) by recycled flue gas/steam in two separate fluidized-bed reactors as a means of separating oxygen from air.

oxidation

$$Me_xO_{y-2}(s) + O_2(g) \rightarrow Me_xO_y(s) \quad (1)$$

reduction

$$Me_xO_y(s) \rightarrow Me_xO_{y-2}(s) + O_2(g) \quad (2)$$

As shown in Figure 1, the reduced metal oxide particles are fed to the oxidation reactor (OR), where air is used to reoxidize them to a higher oxidation state. The oxidized carrier particles are then transported back to the reduction reactor (RR), where oxygen decoupling occurs in the presence of recycled CO_2/steam. The successful implementation of the CLAS process largely depends upon the regenerative nature of the metal oxides used as oxygen carriers. According to Le Chatelier's principle, the redox ability can be best achieved by disturbing the equilibrium partial pressure of oxygen through introducing oxidizing reactant (air for oxidation) and/or inert gases (steam/

Special Issue: 4th (2013) Sino-Australian Symposium on Advanced Coal and Biomass Utilisation Technologies

Received: July 30, 2013
Revised: September 11, 2013
Published: September 11, 2013

dx.doi.org/10.1021/ef401487x | *Energy Fuels* 2014, 28, 173−182

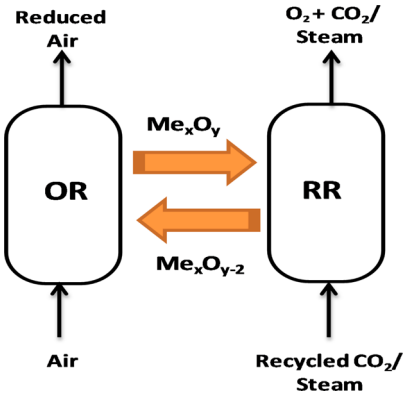

Figure 1. Schematic of the CLAS process.

CO_2 for reduction). In this context, steam/CO_2 works as a carrier gas and also controls the partial pressure of O_2 in the reduction reactor.

The configuration of the CLAS process is similar to the chemical looping oxygen uncoupling (CLOU) process proposed for the solid/gaseous fuel combustion.[12−23] The description of the CLOU process can be found elsewhere.[12−23] However, there is a fundamental difference between CLAS and CLOU processes. In the CLOU process, similar to the CLAS process, oxygen carriers are reduced to release oxygen in the fuel reactor by keeping the actual partial pressure of O_2 below its equilibrium value. However, unlike the CLAS process, released gas-phase oxygen in the fuel reactor then reacts directly with char and volatiles, as it happens in the conventional combustion systems. Also, in the CLOU process, the oxygen concentration at the outlet should be around 4 vol % for ensuring complete combustion of the fuel, while CLAS needs to operate at a larger concentration of around 28 vol % as per oxy-combustion process requirement.

Similar to other typical chemical-looping-based processes, CLAS also faces many challenges, and among them, identifying the efficient and stable oxygen carrier materials is challenging. Cu-, Co-, and Mn-based metal oxides in oxidation pairs of CuO/Cu_2O, Co_3O_4/CoO, and Mn_2O_3/Mn_3O_4 are found to be the most thermodynamically feasible oxygen carrier candidates for CLOU/CLAS processes.[7,10−12] From the literature review, it can be seen that Cu-based oxygen carriers have been studied the most for CLOU-based operations. The reasons behind the interest on CuO/Cu_2O oxygen carriers are the higher oxygen transport capacity, higher reactivity, lesser inventory, and lower raw material costs.[12,13] It is also identified in the literatures that Cu-based oxygen carriers, although as most favorable oxygen carriers, face a number of challenges, e.g., their lower mechanical strength, lower melting point, and serious agglomeration issues.[12,13,15−17] To overcome these challenges, various support materials have been explored.[15−17] Cu-based oxygen carriers supported by either ZrO_2 or $MgAl_2O_4$ have exhibited higher reactivity, greater mechanical strength, and no agglomeration issues.[12,13,15,17,18] A number of oxygen carrier preparation methods, such as mechanical mixing plus pressurized pelletizing, impregnation, spray drying, and freeze granulation, have also been studied.[12,20,21] Except for the synthesized oxygen carriers, a more recent experimental study on Cu-based mineral ore also offers a possibility of using more economic Cu minerals as oxygen carriers for CLOU/CLAS.[22]

Although there is extensive literature reported on identifying chemical stability and mechanical properties of Cu-based oxygen carriers on the SiO_2 support, very few studies in the current literature have focused on determining the reduction and oxidation kinetics of oxygen carriers for CLOU/CLAS applications. Chadda et al.[24] studied the cyclic decomposition of cupric oxide, followed by the oxidation of cuprous oxide in a thermogravimetric analyzer (TGA). The activation energy of the decomposition reaction was found to be 313 kJ/mol in the temperature range of 760−910 °C. The oxidation kinetics was derived at low temperatures in the range of 400−500 °C and, therefore, cannot be applied to chemical-looping-based processes. Eyring et al.[23] in their CLOU-based study, investigated the rate of decomposition of fine CuO powder in a TGA in the temperature range of 750−950 °C and found that the decomposition could be explained by an Arrhenius type of expression and calculated an activation energy of 327 kJ/mol, which was found to be similar to that obtained by Chadda et al.[24] For the oxidation reaction, Eyring et al.[23] observed a decrease in the oxidation rate as a function of the temperature in the interval of 850−950 °C when oxidizing a fine CuO powder in air. It was claimed that this is because, at higher temperatures, the driving force for the reaction, i.e., the difference between the actual oxygen partial pressure and the equilibrium oxygen partial pressure ($P_{O_2} - P_{O_{2,e}}$), will reduce and, thus, a slower rate of reaction may be expected as the temperature increases. The authors used nitrogen as a sweep gas during the decomposition. However, when nitrogen is used to simulate such a condition, decomposition may approach the equilibrium oxygen concentration, thus releasing oxygen at a limited rate, which may be slower than the actual rate in a real CLOU process, where the released oxygen will be consumed by a solid/gaseous fuel. Therefore, Arjmand et al.[25] introduced an excess of devolatilized wood char to a bed of freeze-granulated $CuO/MgAl_2O_4$ particles and calculated the rate of decomposition in the temperature interval of 850−900 °C. The decomposition reaction was modeled using the Avrami−Erofe'ev mechanism, and the kinetic data were obtained using an Arrhenius expression. From the analysis, activation energy of 139.3 kJ/mol was calculated for the decomposition reaction, which was quite lower than the above published values under a N_2-reducing environment. Whitty and Clayton[26] performed decomposition experiments in three types of reactor systems using N_2 and found that the rate of decomposition was independent of the reactor type and also very similar for the three Cu-based oxygen carriers evaluated, with an average activation energy found of 110 kJ/mol. However, they investigated the rate of oxidation for an oxygen carrier of CuO/ZrO_2 as a function of the temperature and oxygen driving force. Although an increase in the oxidation rate was seen when the oxygen partial pressure was increased, the increase in the rate was not as high as expected, indicating the complexity associated with the reaction mechanism. They suggested that physical factors, such as grain growth, grain boundary concentration depletion, and sintering of grains, could also be responsible for the decline in the oxidation rate at high temperatures. The activation energy of the oxidation of 202 kJ/mol was found for this oxygen carrier.[26]

From the above literature review, it can be stated that the published studies on determining kinetics of CuO/SiO_2 oxygen carriers, although they have higher oxygen transport capacity, higher reactivity, and lower inventory requirement, are very limited for CLOU/CLAS processes.[15,17] In a previous study, Adánez-Rubio and his co-authors found that CuO/SiO_2

dx.doi.org/10.1021/ef401487x | *Energy Fuels* 2014, 28, 173−182

exhibits highest reactivity among mechanically mixed oxygen carriers from the experiments performed in a TGA.[15] It has also been observed that Cu oxides do not react with the SiO_2 and have the highest reactivity and oxygen transport capacity.[27] Unfortunately, they have rejected it simply based on the weakness of mechanical strength.[15,17] However, the impregnated oxygen carriers may show relatively high mechanical strength and low attrition rate, leading to a long lifetime.[6,28] Moreover, impregnation is also a cost-effective method to produce oxygen carriers compared to sol−gel, spray drying, or freeze granulation methods. To the best of the authors' knowledge, there is no reported study in the current literature on investigating the kinetics of impregnated CuO/SiO_2 oxygen carriers for CLOU/CLAS processes. Also, there are discrepancies associated with the Cu-based oxygen carrier kinetics in the literature, as mentioned earlier. Looking above, the objective of the current study is to investigate the reactivity and reaction kinetics of CuO/SiO_2 oxygen carriers prepared by a dry impregnation method for CLAS operation.

2. EXPERIMENTAL SECTION

2.1. Preparation of Oxygen Carriers. The copper oxide oxygen carriers used in this study were produced for three distinctive active CuO contents (i.e., 18, 29, and 48 wt %) by a dry impregnation method using SiO_2 as an inert support material and copper nitrate trihydrate as a CuO precursor. Silica was purchased from Grace Davison Discovery Science with a particle size of around 70−200 μm and a surface area of 285−355 m^2/g. Copper nitrate trihydrate was obtained in purum pro analysi (p.a.) grade from Sigma-Aldrich. During preparation, raw silica was dried overnight in an oven at a temperature of 110 °C to remove the pore moisture. To ensure the desired content of CuO in fresh oxygen carriers, stoichiometric copper nitrate trihydrate was dissolved in deionized water to form a volume of nitrate solution equal to the pore volume of silica to be impregnated. Then, this solution was slowly poured to the hot silica binders until wet pasta was obtained. The resultant pasta was dried overnight at 110 °C, followed by calcination at 600 °C for 3 h in a muffle furnace to decompose the copper nitrate to copper oxide entirely. The above steps were repeated until the desired content of copper oxide was achieved. Finally, all calcined samples were sintered at 950 °C for 6 h. After calcination, the oxygen carriers in the particle size of 106−150 μm were sieved out for experiment and further kinetic analysis. Also, to investigate the effect of the particle size on reactivity, a batch of fresh samples were sieved into different particle size ranges, i.e., 53−75, 75−90, 90−125, and 125−150 μm.

2.2. Experimental Apparatus. The reactivity tests for CuO/SiO_2 were carried out in a TA-Q50 TGA. The schematic of TGA is illustrated in Figure 2. It consists of a furnace, gas switching unit, and microbalance unit. In application, the microbalance unit requires an empty sample holder for balancing the sample holder to accurately derive the actual sample weight. During experiment, the oxygen carriers were placed in the sample holder (i.e., 10 mm in diameter and 2 mm height) and the furnace would then be lifted automatically for driving the sample holder into the temperature stable zone. Nitrogen was used for reduction, while air or diluted air was taken as the oxidizing gas for oxidation. The flow rate of reacting gas was regulated through the mass flow controller (MFC) equipped in TGA and varied from 60 to 180 mL/min. Moreover, a separate flow of inert gas, i.e., N_2, at a rate of 60 mL/min, was fed into the microbalance the entire time for the protection of the microbalance. A typical reaction time of 30 min was set for both reduction and oxidation processes. The weight and furnace temperature were logged by the data acquisition system of TGA. All of the experiments were conducted at isothermal conditions at the temperature range of 800−975 °C under reduction−oxidation cyclic conditions. The sample was heated to the desired temperature in an air environment at 20 °C/min heating rate and then exposed to the cyclic conditions of reduction and oxidation. Generally, five reduction−oxidation cycles were carried out for all runs.

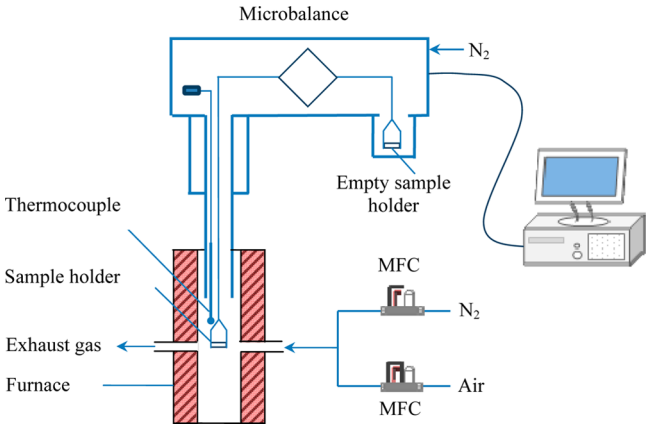

Figure 2. Schematic of the TGA.

3. REACTION MECHANISM DESCRIPTION

The conversion of the oxygen carrier during reduction and oxidation was calculated according to the following equations:

$$\alpha_{red} = \frac{m_{ox} - m_t}{m_{ox} - m_{red}} \quad \text{for reduction} \tag{3}$$

$$\alpha_{ox} = \frac{m_t - m_{red}}{m_{ox} - m_{red}} \quad \text{for oxidation} \tag{4}$$

where α_{red} and α_{ox} are the oxygen carrier conversions during reduction and oxidation, respectively, while m_{ox}, m_{red}, and m_t represent the oxygen carrier weight at the fully oxidized state, the entirely reduced status, and the actual weight during test, respectively.

The reduction of cupric oxide oxygen carriers is based on the forward reaction of $4CuO \leftrightarrow 2Cu_2O + O_2$. This oxygen-released process is similar to those thermal decomposition reactions of some other metal oxides and dehydrated processes reported in the literature.[29−31] Therefore, from the well-known equation of solid conversion for thermal decomposition, a general equation could be derived for both reduction and oxidation reactions as

$$\frac{d\alpha}{dt} = kf(\alpha)(C - C_{eq})^{n_*} \tag{5}$$

wherein the function $f(\alpha)$ is determined by the reaction mechanism, t is the reaction time, k is the reaction rate constant following the Arrhenius-type equation of

$$k = A \exp\left(-\frac{E}{RT}\right) \tag{6}$$

where A, E, R, and T are the pre-exponential factor, activation energy, gas constant, and reaction temperature, respectively.

Exponent n_* is the reaction order. Because the reduction of cupric oxide is a thermal decomposition process, the value of n_* becomes zero. As for the oxidation process, oxygen is present as in the reactive gas (i.e., air); thus, n_* will have a non-zero value, which should be determined experimentally. C and C_{eq} will stand for the oxygen concentration used for oxidation and the equilibrium oxygen concentration used for cupric oxide decomposition at tested temperatures, respectively. Here, C_{eq} can be calculated from the equilibrium oxygen partial pressure,

dx.doi.org/10.1021/ef401487x | Energy Fuels 2014, 28, 173−182

$P_{O_2,e}$, which is determined by the Gibbs free energy of cupric oxide decomposition as

$$P_{O_2,e} = \exp\left(-\frac{\Delta G}{RT}\right) \quad (7)$$

In this study, Gibbs free energy, ΔG, was derived on the basis of the empirical equation developed by Kubaschewski et al.[32] for cupric oxide decomposition as

$$\Delta G = 292 + 0.051T \log T - 0.37T \quad (298 \le T \le 1323\ \text{K}) \quad (8)$$

Given that $(C - C_{eq})^{n^*}$ in eq 5 is a function of the temperature T for oxidation or becomes 1 for reduction, an integral form of the equation, which is more useful, can be derived for eq 5 as follows:

$$G(\alpha) = \int_0^\alpha \frac{1}{f(\alpha)} d\alpha = \int_0^t k(C - C_{eq})^{n*} dt = k(C - C_{eq})^{n*} t \quad (9)$$

Various expressions of $G(\alpha)$ can be obtained via different reaction mechanisms.[29−31,33,34] Table 1 has summarized those equations to be determined in this kinetic study.

Table 1. Summarization of $G(\alpha)$ Equations for Different Reaction Mechanisms[a]

reaction mechanism	$G(\alpha)$	reaction mechanism	$G(\alpha)$
D1	α^2	A3	$[-\ln(1-\alpha)]^{1/3}$
D2	$(1-\alpha)\ln((1-\alpha)+\alpha$	R2	$1-(1-\alpha)^{1/2}$
D3	$[1-(1-\alpha)^{1/3}]^2$	R3	$1-(1-\alpha)^{1/3}$
D4	$1-2\alpha/3-(1-\alpha)^{2/3}$	P1	α
C1	$-\ln(1-\alpha)$	P2	$\alpha^{1/2}$
C2	$(1-\alpha)^{-1}-1$	P3	$\alpha^{1/3}$
A2	$[-\ln(1-\alpha)]^{1/2}$	P4	$\alpha^{1/4}$

[a]D1, one-dimensional diffusion; D2, two-dimensional diffusion; D3, three-dimensional diffusion (Jandar function); D4, three-dimensional diffusion (G-B function); C1, first-order chemical reaction; C2, second-order chemical reaction; An, Avrami−Erofe'ev random nucleation and subsequence growth, where n = 2 or 3; Rn, phase boundary reaction, where n = 2 or 3; and Pn, Mampel power law, where n = 1, 2, 3, or 4.

4. RESULTS AND DISCUSSION

During a reduction−oxidation cycle, a Cu-based oxygen carrier will initially release oxygen through cupric oxide decomposition, and therefore, the weight of the oxygen carrier in the TGA will substantially decrease until it attains a constant weight at the end of decomposition. Following the oxidation process, cuprous oxide will be oxidized back to cupric oxide, and as such, the weight of oxygen carrier sample will increase. Such a reduction−oxidation cycle was generally repeated 5 times for all experiments to obtain stable operation with an increasing cycle number. A typical test result for 18 wt % CuO/SiO_2 at 900 °C has been shown in Figure 3. It can be observed that the first reduction−oxidation cycle was unstable compared to the following cycles. In this study, only fifth cycle experimental data were used for oxygen carrier conversion calculations.

In general, three types of resistances may potentially affect the gas−solid reaction in chemical looping processes, i.e., gas

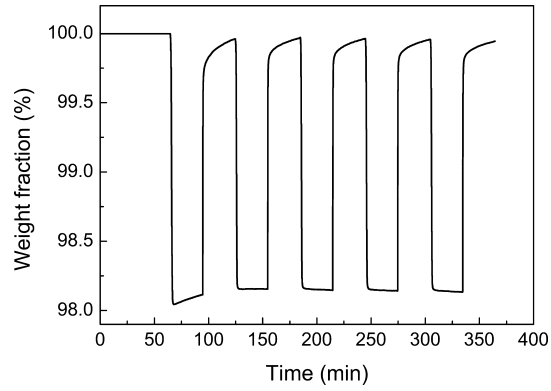

Figure 3. Weight fraction for the 18 wt % CuO/SiO_2 oxygen carrier during five consecutive reduction−oxidation cycle tests conducted at 900 °C.

film resistance, particle layer resistance, and chemical reaction resistance. To evaluate the effect of gas film resistance and particle layer resistance on the reactivity of CuO/SiO_2, a series of experiments have been carried out by varying the gas flow rate and sample loading weight in the range of 60−180 mL/min and 10−30 mg, respectively, as well as altering the particle size of oxygen carriers from 53−75 to 125−150 μm.

Figure 4 illustrates the effect of the gas flow rate on oxygen carrier conversion during oxidation measured for the oxygen

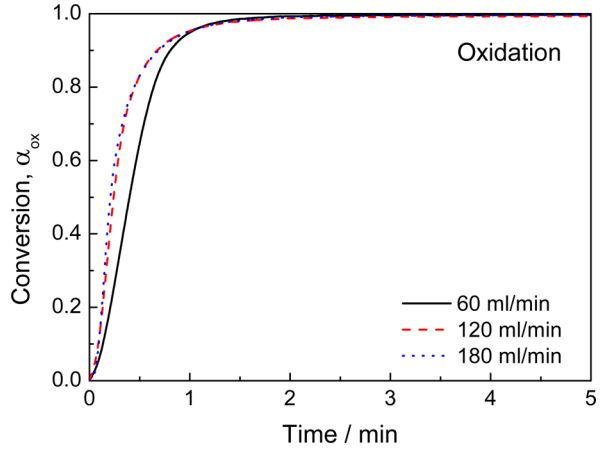

Figure 4. Effect of the gas flow rate on the oxidation at 900 °C for the 48 wt % CuO/SiO_2 oxygen carrier.

carrier of 48 wt % CuO/SiO_2 at 900 °C. Clearly, it can be seen that increasing gas flow rate to 120 mL/min may significantly reduce the influence of external gas film resistance. The same results were also obtained for the reduction reaction (not shown). The results for sample loading were also analogous to the gas flow rate. It was observed that, by decreasing the sample loading weight to as low as 12 mg, gas diffusion problems can be minimized (not shown). On the other hand, less effect of the particle layer resistance was observed for CuO/SiO_2 oxygen carriers for a particle size larger than 75 um, as shown in Figure 5 for reduction. As above, similar results for particle layer resistance were obtained for the oxidation reaction (not shown). As a result, the gas flow rate, loading weight, and particle size were optimized as approximately 195 mL/min, 10 mg, and 106−150 μm, respectively, for further experiments for deriving chemical kinetics.

dx.doi.org/10.1021/ef401487x | Energy Fuels 2014, 28, 173−182

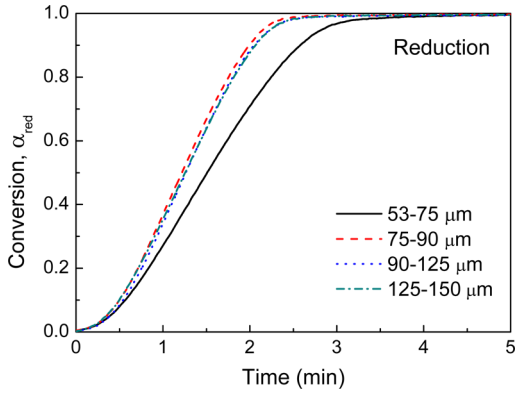

Figure 5. Effect of the oxygen carrier particle size on the reduction at 900 °C obtained for the 48 wt % CuO/SiO_2 oxygen carrier.

Apart from above, another important aspect required to be considered is to find the influence of the CuO content in the oxygen carriers on their reactivity. The effect of the CuO content in CuO/SiO_2 oxygen carriers on solid conversion during reduction has been presented in Figure 6. As seen, a higher content of CuO, i.e., 48 wt %, has caused the decline in the reduction rate by approximately 0.53 to a rate of 0.47 min^{-1}, in comparison to 1 min^{-1} for 18 wt % CuO/SiO_2. However, the effect was found to be less between 18 and 29 wt %. The decline of the reduction rate in the case of 48 wt % CuO/SiO_2 is very likely due to the inner diffusion resistance and possible agglomeration of CuO. It has been reported in the literature that agglomeration can occur because of many reasons, e.g., the sintering temperature, type of inert material, and high copper oxide content.[14,15,17,28] Similar results for active CuO content were obtained for the oxidation reaction (not shown).

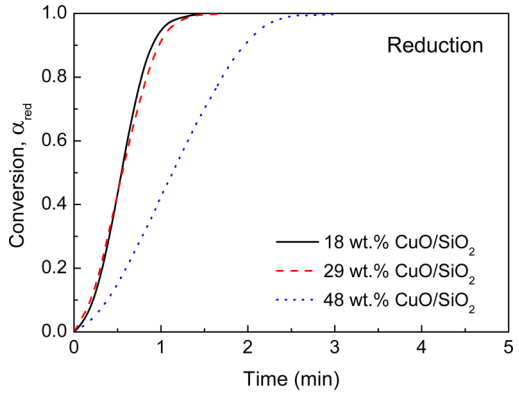

Figure 6. Oxygen carrier conversion during reduction at 900 °C versus time for CuO/SiO_2 oxygen carriers with varying CuO loading content.

To determine the underlying reason for the decline of the reduction rate occurring in this study, surface morphology for the fresh oxygen carrier samples with 18 and 48 wt % CuO was analyzed though scanning electron microscopy (SEM). The images at 2000× magnification are shown in Figure 7. Copper oxide was found to be distributed largely around the surface of SiO_2 for both cases. However, a very intense and thicker layer of CuO has been found in the case of 48 wt % CuO. From this, it can be assumed that this thick layer of CuO will significantly increase the agglomeration tendency of 48 wt % CuO/SiO_2. Furthermore, the inner diffusion resistance through this thick layer can also be expected to be higher. The above suggests the use of possible lower CuO loading on SiO_2. Therefore, 18 wt % CuO/SiO_2 is selected for the determination of chemical kinetics, even though authors noticed that the reaction rate for CuO/SiO_2 was not affected up to 29 wt % loading.

As noted earlier, eq 9 has been derived for analyzing the reduction and oxidation kinetics. It offers the correlation that $G(\alpha)$ for a possible reaction mechanism from Table 1 and time t should follow. Because $k(C - C_{eq})^{n^*}$ is temperature-dependent, the most appropriate $G(\alpha)$ should give the best fitting against time t for either the reduction or oxidation from an isothermal test. Multicycle tests of five reduction−oxidation tests have been conducted for 18 wt % CuO/SiO_2 at the temperature range of 800−975 °C with a temperature gradient of 25 °C. $G(\alpha)$ was calculated for reduction and oxidation according to all reaction mechanisms listed in Table 1. For comparison purposes, the R^2 values of the least-squares linear fitting for the temperature from 800 to 975 °C were summarized for all reaction mechanisms in Tables 2 and 3 for reduction and oxidation, respectively.

From Table 2, it can be seen that the Avrami−Erofe'ev random nucleation and subsequence growth model with $n = 2$, i.e., A2, was found to achieve better overall fitting than others in the temperature range of 800−975 °C for reduction (see the R^2 values listed in Table 2). The reaction rate constant k was then determined from the A2 model for the reduction process. Given that, for the reduction process, $k(C - C_{eq})^{n^*}$ in eq 9 was

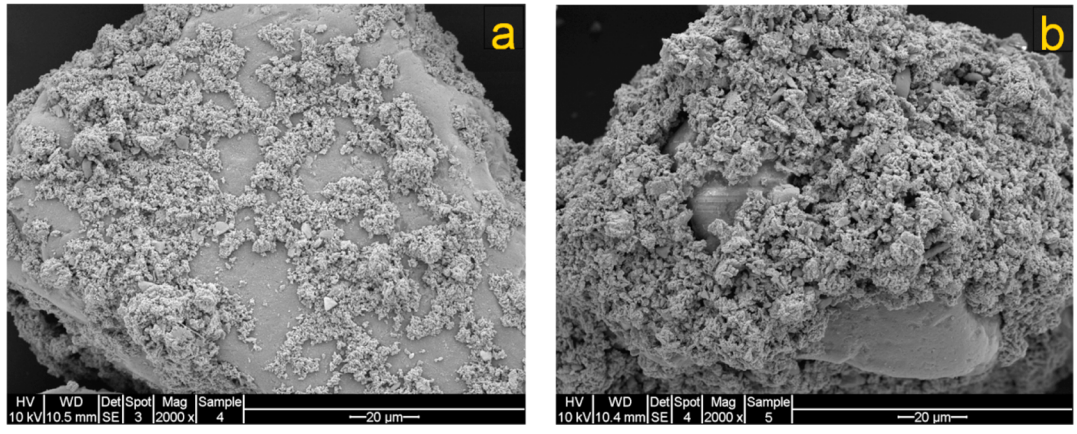

Figure 7. SEM images at 2000× magnification for the fresh oxygen carriers of (a) 18 wt % CuO/SiO_2 and (b) 48 wt % CuO/SiO_2.

dx.doi.org/10.1021/ef401487x | Energy Fuels 2014, 28, 173−182

Table 2. R^2 Values for Fitting Different Reaction Mechanisms Based on the Oxygen Carrier Conversion during Reduction at the Temperature Range of 800−975 °C for the 18 wt % CuO/SiO_2 Oxygen Carrier

T (°C)	D1	D2	D3	D4	C1	C2	A2	A3	R2	R3	P1	P2	P3	P4
800	0.8244	0.763	0.6758	0.7344	0.8582	0.6094	0.9917	0.8077	0.9423	0.9189	0.9837	0.8625	0.3825	−0.405
825	0.8034	0.7451	0.6616	0.7177	0.8342	0.5909	0.9969	0.8926	0.9199	0.8951	0.9648	0.925	0.5842	−0.017
850	0.7678	0.7041	0.5961	0.6698	0.7344	0.3912	0.9604	0.989	0.8604	0.826	0.9221	0.9732	0.8454	0.5804
875	0.7583	0.7008	0.6031	0.6698	0.7311	0.4195	0.9468	0.9916	0.8453	0.814	0.9024	0.971	0.8756	0.6372
900	0.8644	0.8088	0.6938	0.7745	0.8058	0.4188	0.9874	0.9644	0.9316	0.9012	0.9696	0.9325	0.7461	0.4898
925	0.8413	0.7835	0.6732	0.7497	0.799	0.4395	0.9901	0.9556	0.9194	0.889	0.9588	0.898	0.6065	0.1818
950	0.8086	0.7504	0.6426	0.7169	0.7615	0.4209	0.9695	0.9905	0.8857	0.8534	0.9339	0.945	0.7884	0.5321
975	0.7661	0.699	0.5618	0.6571	0.6644	0.2916	0.9182	0.9944	0.837	0.7928	0.9054	0.9723	0.9134	0.7755

Table 3. R^2 Values for Fitting Different Reaction Mechanisms Based on the Oxygen Carrier Conversion during Oxidation at the Temperature Range of 800−975 °C for the 18 wt % CuO/SiO_2 Oxygen Carrier

T (°C)	D1	D2	D3	D4	C1	C2	A2	A3	R2	R3	P1	P2	P3	P4
800	0.7253	0.7057	0.6851	0.6988	0.8866	0.8354	0.9993	0.9374	0.9092	0.9019	0.9291	0.9892	0.9014	0.8052
825	0.8378	0.8161	0.7912	0.8078	0.9338	0.9009	0.9817	0.8541	0.9627	0.9579	0.9742	0.9493	0.7843	0.5979
850	0.8496	0.8218	0.7878	0.8106	0.9359	0.8649	0.9901	0.9081	0.9585	0.952	0.9719	0.9548	0.833	0.6696
875	0.8627	0.8335	0.7963	0.8213	0.9229	0.856	0.9786	0.8657	0.9605	0.9544	0.9701	0.9129	0.7414	0.5486
900	0.8786	0.8516	0.8166	0.8402	0.9531	0.8825	0.9789	0.8529	0.9725	0.9673	0.9812	0.9235	0.7443	0.5212
925	0.8294	0.7975	0.7591	0.7848	0.9313	0.8486	0.9853	0.8274	0.9594	0.9511	0.9777	0.9357	0.7045	0.4122
950	0.8035	0.7761	0.745	0.7657	0.937	0.873	0.9631	0.7323	0.9608	0.9536	0.9784	0.9096	0.607	0.2548
975	0.9081	0.8743	0.8288	0.8595	0.9722	0.877	0.9192	0.5938	0.9935	0.9886	0.9955	0.7649	0.2869	−0.28

simplified to k because of the zero value of n_*, the slope from fitting the A2 model with time t then provides the value of k. Figure 8 shows the fittings between the A2 model and time t for

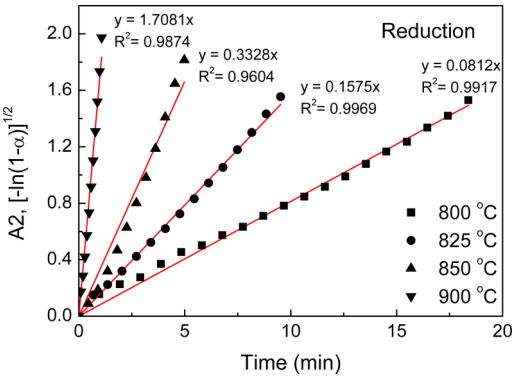

Figure 8. Plots for the reaction rate constant k determination from Avrami−Erofe'ev random nucleation and subsequence growth model with n = 2, i.e., A2 model, for the reduction of the 18 wt % CuO/SiO_2 oxygen carrier under a N_2 environment. The continuous lines are the fitting results between the A2 model and time using the linear least-squares regression method. Symbols represent the A2 model calculated from the oxygen carrier conversion during reduction at corresponding temperatures.

the typical experiments conducted at 800, 825, 850, and 900 °C. The values of 0.0812, 0.1575, 0.3328, and 1.7081 were obtained for the reaction rate constants at 800, 825, 850, and 900 °C, respectively. On the basis of this, an Arrhenius type of plot has been constructed, as shown in Figure 9. Consequently, the kinetic parameters, such as activation energy E and pre-exponential factor A, can be determined from the slope and intercept of the plot in Figure 9.

From above, the reduction process is characterized by an apparent activation energy of 315 kJ/mol with pre-exponential factor $A = 1.595 \times 10^{14}$ min^{-1} in the temperature range of 800−900 °C and 176 kJ/mol with $A = 1.189 \times 10^{8}$ min^{-1} for

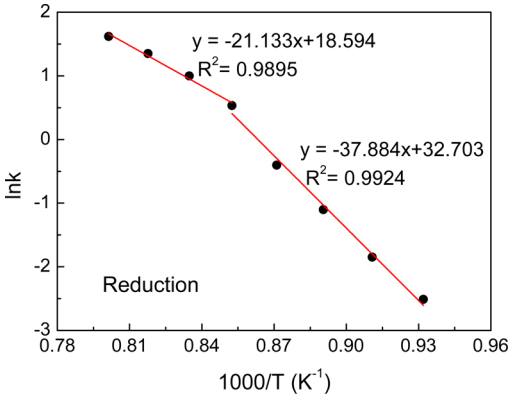

Figure 9. Arrhenius plot for the reduction reaction of the 18 wt % CuO/SiO_2 oxygen carrier under a N_2 environment.

the temperatures exceeding 900 °C. Interestingly, the published study on determining the CuO reduction kinetics has established such two different temperature regimes.[35] The activation energy of reduction at low temperature determined in the current study, i.e., 315 kJ/mol, is in good agreement with the reported value of 322 kJ/mol for the pure CuO decomposition with a particle size around 10 μm in the temperature range of 760−910 °C.[24] Authors believe that a diffusional effect caused by the thermodynamic properties of CuO may be more intense at lower temperatures compared to the higher temperatures. According to the calculations from eqs 7 and 8, the equilibrium oxygen partial pressure will increase from a very low value of 0.11 to 7.19% (i.e., ∼65 times higher) as the temperature increases from 800 to 975 °C. For reduction, the equilibrium oxygen pressure can be more readily reached at low temperatures compared to that under high temperatures. Although the gas flow rate is selected as high as possible for the experiments to reduce the diffusion effect, the equilibrium pressure can still be attained at the boundaries surrounding the unreacted grains inside the CuO/SiO_2 particles. Once the equilibrium is reached, the reduction rate

dx.doi.org/10.1021/ef401487x | Energy Fuels 2014, 28, 173−182

will be significantly reduced because of the transportation difficulties for the produced oxygen, viz., diffusion effect. However, such a diffusion effect can be expected to decrease with an increasing temperature because of the increase in the equilibrium oxygen partial pressure. Therefore, the decrease in activation energy (i.e., 176 kJ/mol) at temperatures higher than 900 °C should be the result of combined effects of diffusion/equilibrium oxygen partial pressure and structural transformations. Also, the agglomeration of the active metal oxide in CuO/SiO_2 prepared by a dry impregnation method, as discussed earlier, possibly exists, in particular, for higher temperatures, leading to a sintering of the grain size. As a result, the oxygen diffusion resistance may increase during reduction, finally reflected by the observed reduced activation energy. Similarly, two different temperature regimes for kinetics can be found for the reduction of hematite.[33,34]

Predictions were also performed for the reduction using the obtained kinetic parameters. The typical prediction results (solid line) for oxygen carrier conversion during reduction at temperatures of 800, 825, 850, 875, 900, and 975 °C are shown in Figure 10, along with experimental data (dot points). A good agreement between predictions and experiment has been achieved for all temperatures.

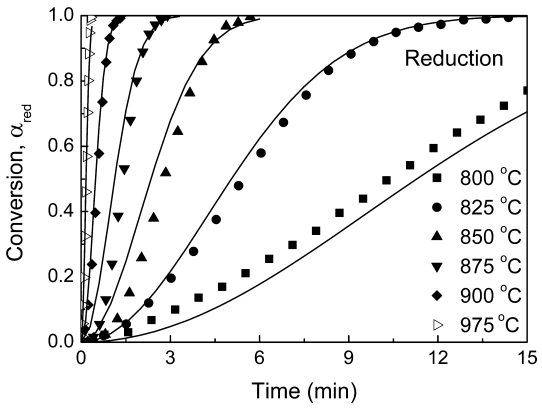

Figure 10. Oxygen carrier conversion during reduction under a N_2 environment at 800, 825, 850, 875, 900, and 975 °C versus time for the 18 wt % CuO/SiO_2 oxygen carrier. The continuous lines represent the A2 model prediction using the kinetic data of E = 315 kJ/mol and $A = 1.595 \times 10^{14}$ min^{-1} and E = 176 kJ/mol and $A = 1.189 \times 10^{8}$ min^{-1} corresponding to the temperature range of 800–900 °C and temperature of 975 °C, respectively.

For the oxidation process, A2, R2, and P1 have been found as the most suitable reaction mechanisms based on their R^2 values summarized in Table 3. Because the R^2 values of these three models are very close to each other, all of these three models have all been studied further in detail. To identify the most suitable model, the R^2 values were obtained for fitting these three models against t while further increasing oxygen carrier conversion for oxidation. As an example, Table 4 lists the R^2 values for increasing oxygen carrier conversion obtained for a typical oxidation at 900 °C, for which the R2 model provided the best fit. Similar findings were also found for other temperatures (not shown). It has been observed that the R2 model performs better than A2 and P1 in terms of Arrhenius plot linearity and the prediction of oxygen carrier conversion for oxidation and, therefore, was selected for further deriving oxidation kinetics.

Table 4. R^2 Values for Fitting A2, R2, and P1 Reaction Mechanisms upon Increasing Oxygen Carrier Conversion during Oxidation at 900 °C for the 18 wt % CuO/SiO_2 Oxygen Carrier

α_{ox}	A2	R2	P1
0.6786	0.9789	0.9725	0.9812
0.7976	0.9377	0.9844	0.967
0.8619	0.9066	0.979	0.9342
0.9	0.9528	0.9658	0.8879
0.9366	0.9437	0.952	0.837

Figure 11 displays the fittings between the R2 model and time t for the typical experiments conducted at 825, 925, 950,

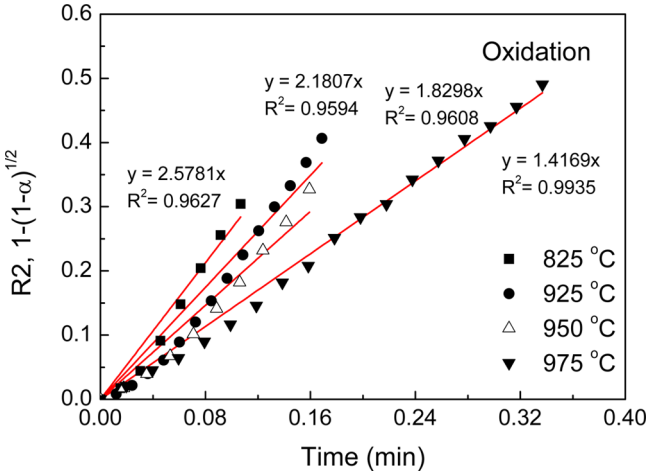

Figure 11. Plots for the $k(C - C_{eq})^{n^*}$ determination from the phase boundary reaction model with n = 2, i.e., R2 model, for the oxidation of the 18 wt % CuO/SiO_2 oxygen carrier under an air environment. The continuous lines are the fitting results between the R2 model and time using the linear least-squares regression method. Symbols represent the R2 model calculated from the oxygen carrier conversion during oxidation at corresponding temperatures.

and 975 °C. The slopes in Figure 11 from the linear least-squares regression represent the value of $k(C - C_{eq})^{n^*}$ at corresponding temperatures. A series of such values of $k(C - C_{eq})^{n^*}$ can be obtained for all oxidation experiments conducted at the temperature range of 800–975 °C. However, unlike the thermal decomposition reaction of reduction, oxidation is a type of gas–solid chemical reaction between oxygen and cuprous oxide. The reaction order n_* of oxidation must be determined before obtaining the reaction rate constant k for deriving the Arrhenius plot. A method as applied in the previous studies[3,4] has been adopted. According to this method, $\ln[k(C - C_{eq})^{n^*}]$ values were plotted against the $\ln(C - C_{eq})$ values for the oxidation processes. Through the linear least-squares fitting of such a plot, the values of $\ln k$ and n_* have been obtained as the intercept and slope, respectively. It should be noted that k is a temperature-dependent variable and n_* is a constant. Two sets of tests were conducted at 850 and 950 °C. The values of $C - C_{eq}$ were varied by diluting air with N_2 to keep $P_{O_2} - P_{O_2,e}$ at three constant values of 0.07, 0.11, and 0.15. Correspondingly, the values of $k(C - C_{eq})^{n^*}$ were obtained using the same method as described earlier for these additional two sets of tests. The resulting plots of $\ln[k(C - C_{eq})^{n^*}]$ versus $\ln(C - C_{eq})$ for oxidation are shown in Figure 12. The values of n_* are found to be 0.5061 and 0.5097 for temperatures of 850

dx.doi.org/10.1021/ef401487x | Energy Fuels 2014, 28, 173–182

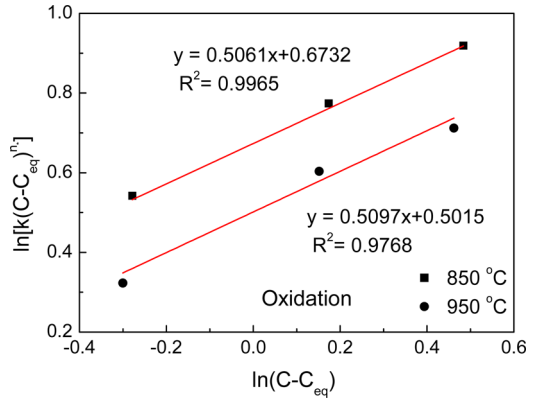

Figure 12. Plots of $\ln[k(C - C_{eq})^{n^*}]$ versus $\ln(C - C_{eq})$ at 850 and 950 °C for the oxidation reaction order determination for the 18 wt % CuO/SiO_2 oxygen carrier. $P_{O_2} - P_{O_2,e}$ = 0.07, 0.11, and 0.15.

and 950 °C, respectively (see the slope shown in Figure 12). Both of these values are very close to the mole ratio of Cu_2O/O_2 for the oxidation reaction of reduced CuO/SiO_2 oxygen carriers, i.e., $^1/_2$. Therefore, the oxidation reaction order n_* was finally considered as $^1/_2$. On the other hand, from the exponent of the intercept, the reaction rate constant k can also be calculated as 1.959 and 1.651 $m^{3/2}$ $mol^{-1/2}$ min^{-1} for temperatures of 850 and 950 °C, respectively. Once n_* is obtained, the reaction rate constant k can be calculated for oxidation at the temperature range of 800−975 °C from the values of $k(C - C_{eq})^{n^*}$. The values of k calculated for 850 and 950 °C are 1.96 and 1.688, respectively. It can be observed they are in agreement with the values of 1.959 and 1.651 calculated earlier while determining the reaction order. Such observation confirms the suitability of the adopted method[3,4] for determining n_* in this study.

Arrhenius plot for the oxidation kinetics has been constructed for the temperature range of 800−975 °C, as illustrated in Figure 13. It can be noticed that the Arrhenius

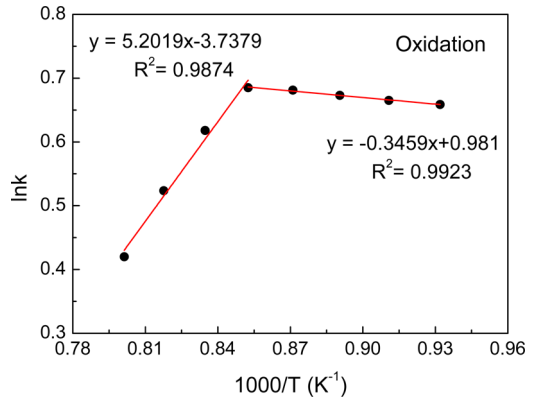

Figure 13. Arrhenius plot for the oxidation reaction of the 18 wt % CuO/SiO_2 oxygen carrier under an air environment.

plot for oxidation follows a similar trend to the reduction process. Two distinct temperature zones were also observed. More specifically, for oxidation at the higher temperature range of 900−975 °C, the slope of the Arrhenius plot even becomes positive, leading to a negative value for activation energy. The activation energy and pre-exponential factor calculated from the plots in Figure 13 are 3 kJ/mol and 2.67 $m^{3/2}$ $mol^{-1/2}$ min^{-1} and −43 kJ/mol and 0.024 $m^{3/2}$ $mol^{-1/2}$ min^{-1} corresponding to the temperatures in ranges of 800−900 and 900−975 °C, respectively. It must be pointed out that negative activation energy has already been reported in some studies on pure cuprous oxide oxidation at the temperatures higher than 900 °C and ranges from −63 to −45 kJ/mol, irrespective of the selected oxidation reaction mechanisms.[35,36] The reasons for the negative value of oxidation activation energy at a higher temperature range may be similar to the decrease of the activation energy for the reduction at high temperatures, as discussed earlier, i.e., the intense diffusional barrier because of the sintering effect at high temperatures and the thermodynamic limitations of cuprous oxide itself. However, the thermodynamic effect will be reverse for oxidation compared to the reduction. For reduced CuO/SiO_2 particles, oxidation can proceed only when the actual oxygen partial pressure is higher than the equilibrium oxygen partial pressure. Thereafter, it may be concluded that the driving force for oxidation is largely determined by the difference between the actual oxygen partial pressure and equilibrium oxygen partial pressure, viz., $P_{O_2} - P_{O_2,e}$, at given temperatures. Because the equilibrium oxygen partial pressure is much higher for the higher temperature range of 900−975 °C, viz., 1.4−7.19%, compared to 0.11−1.4% for the lower temperature range of 800−900 °C, the driving force for oxygen species to unreacted cuprous oxide is expected to be significantly smaller at higher temperatures when air (assuming 21 vol % O_2) is used as oxidizing gas. It should be noted that the balance gas flow of N_2 at 60 mL/min for protecting the TGA balance that passed over the oxygen carrier samples during the tests may also be responsible for the much lesser actual oxygen partial pressure than 0.21. As a consequence, the oxidation rate can be reduced with an increasing temperature, in particular, at a higher temperature range.

Panels a and b of Figure 14 show the oxygen carrier conversion during oxidation at 800, 900, 925, 950, and 975 °C with air as the oxidizing gas and the solid conversion for oxidation at 850 °C with a varying oxygen content by keeping $P_{O_2} - P_{O_2,e}$ at three constant values of 0.07, 0.11, and 0.15, respectively, along with the corresponding predictions using the obtained oxidation kinetic parameters. As seen in Figure 14a, the oxidation rate generally decreases with an increasing temperature when air is used as the oxidizing gas. Similar to the earlier discussion, the main reason behind this is the combined effects of diffusion/equilibrium oxygen partial pressure and structural transformations. It is observed from Figure 14b that the oxidation rate will also decrease with reducing the actual oxygen partial pressure. From both panels a and b of Figure 14, the R2 reaction mechanism with obtained kinetics agrees well with the experimental results up to a conversion of 0.8, regardless of the oxidation temperature and actual oxygen partial pressure.

5. CONCLUSION

In the current study, reaction mechanisms have been identified for the redox reaction of CuO/SiO_2 oxygen carriers prepared by a dry impregnation method. The reduction and oxidation behavior was investigated under N_2 and air separately for the temperature range of 800−975 °C in a TGA. The effects of active copper oxide loading content on the support, gas film resistance, and particle layer resistance on reduction and oxidation processes have been quantified, and typical test conditions, viz., 180 mL/min gas flow rate, 10 mg sample

dx.doi.org/10.1021/ef401487x | Energy Fuels 2014, 28, 173−182

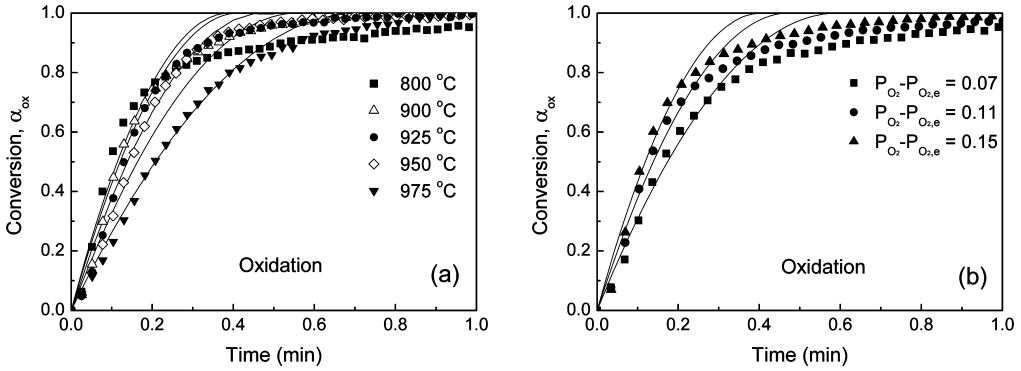

Figure 14. Oxygen carrier conversion during oxidation (a) at 800, 900, 925, 950, and 975 °C under an air environment and (b) for varying the oxygen content by keeping $P_{O_2} - P_{O_2,e}$ = 0.07, 0.11, and 0.15 at 850 °C as a function of time for the 18 wt % CuO/SiO_2 oxygen carrier. The continuous lines represent the R2 model prediction using the kinetic data of E = 3 kJ/mol and A = 2.67 $m^{3/2}$ $mol^{-1/2}$ min^{-1} and E = −43 kJ/mol and A = 0.024 $m^{3/2}$ $mol^{-1/2}$ min^{-1} corresponding to the temperature ranges of 800−900 and 925−975 °C, respectively.

loading, and particle size of 106−150 μm, have been selected for TGA tests for deriving kinetic parameters. The reduction rate was found to increase gradually with an increase in the temperature, while in contrast, a drop in the oxidation rate was observed. The reaction mechanisms for reduction and oxidation processes have been identified for the 18 wt % CuO/SiO_2 oxygen carrier at the temperature range of 800−975 °C. Results indicate that the Avrami−Erofe'ev random nucleation and subsequence growth A2 model and phase boundary reaction R2 mechanism are most suitable for reduction and oxidation, respectively. For the reduction process, the activation energy and pre-exponential factor were determined as 315 kJ/mol and 1.595×10^{14} min^{-1}, respectively, for the temperature range of 800−900 °C, while for the higher temperature range of 900−975 °C, the values of 176 kJ/mol and 1.189×10^{8} min^{-1} were obtained. For the oxidation process, the activation energy and pre-exponential factor were found to be 3 kJ/mol and 2.67 $m^{3/2}$ $mol^{-1/2}$ min^{-1} and −43 kJ/mol and 0.024 $m^{3/2}$ $mol^{-1/2}$ min^{-1}, corresponding to the temperature range of 800−900 and temperatures above 900 °C, respectively.

AUTHOR INFORMATION

Corresponding Author

*E-mail: behdad.moghtaderi@newcastle.edu.au.

Notes

The authors declare no competing financial interest.

ACKNOWLEDGMENTS

The authors gratefully acknowledge the financial support provided by the University of Newcastle (Australia), Coal Innovation NSW, and Xstrata Coal Pty Ltd. for the present study.

REFERENCES

(1) Brown, T. A.; Dennis, J. S.; Scott, S. A.; Davidson, J. F.; Hayhurst, A. N. Gasification and chemical-looping combustion of a lignite char in a fluidized bed of iron oxide. *Energy Fuels* **2010**, *24*, 3034−3048.

(2) Buhre, B. J. P.; Elliott, L. K.; Sheng, C. D.; Gupta, R. P.; Wall, T. F. Oxy-fuel combustion technology for coal-fired power generation. *Prog. Energy Combust. Sci.* **2005**, *31* (4), 283−307.

(3) Moghtaderi, B.; Song, H. Reduction properties of physically mixed metallic oxide oxygen carriers in chemical looping combustion. *Energy Fuels* **2010**, *24* (10), 5359−5368.

(4) Song, H.; Doroodchi, E.; Moghtaderi, B. Redox characteristics of Fe−Ni/SiO_2 bimetallic oxygen carriers in CO under conditions pertinent to chemical looping combustion. *Energy Fuels* **2011**, *26* (1), 75−84.

(5) Abad, A.; Mattisson, T.; Lyngfelt, A.; Ryden, M. Chemical-looping combustion in a 300 W continuously operating reactor system using a manganese-based oxygen carrier. *Fuel* **2006**, *85* (9), 1174−1185.

(6) de Diego, L. F.; Gayan, P.; Garcia-Labiano, F.; Celaya, J.; Abad, M.; Adanez, J. Impregnated CuO/Al_2O_3 oxygen carriers for chemical-looping combustion: Avoiding fluidized bed agglomeration. *Energy Fuels* **2005**, *19* (5), 1850−1856.

(7) Shah, K.; Moghtaderi, B.; Zanganeh, J.; Wall, T. Integration options for novel chemical looping air separation (ICLAS) process for oxygen production in oxy-fuel coal fired power plants. *Fuel* **2013**, *107*, 356−370.

(8) Shah, K.; Moghtaderi, B.; Wall, T. Effect of flue gas impurities on the performance of a chemical looping based air separation process for oxy-fuel combustion. *Fuel* **2013**, *103*, 932−942.

(9) Smith, A. R.; Klosek, J. A review of air separation technologies and their integration with energy conversion processes. *Fuel Process. Technol.* **2001**, *70* (2), 115−134.

(10) Moghtaderi, B. Application of chemical looping concept for air separation at high temperatures. *Energy Fuels* **2010**, *24*, 190−198.

(11) Shah, K.; Moghtaderi, B.; Wall, T. Selection of suitable oxygen carriers for chemical looping air separation: A thermodynamic approach. *Energy Fuels* **2012**, *26* (4), 2038−2045.

(12) Mattisson, T.; Lyngfelt, A.; Leion, H. Chemical-looping with oxygen uncoupling for combustion of solid fuels. *Int. J. Greenhouse Gas Control* **2009**, *3* (1), 11−19.

(13) Abad, A.; Adánez-Rubio, I.; Gayán, P.; García-Labiano, F.; de Diego, L. F.; Adánez, J. Demonstration of chemical-looping with oxygen uncoupling (CLOU) process in a 1.5 kW_{th} continuously operating unit using a Cu-based oxygen carrier. *Int. J. Greenhouse Gas Control* **2012**, *6*, 189−200.

(14) Adanez, J.; Abad, A.; Garcia-Labiano, F.; Gayan, P.; de Diego, L. F. Progress in chemical-looping combustion and reforming technologies. *Prog. Energy Combust. Sci.* **2012**, *38* (2), 215−282.

(15) Adánez-Rubio, I.; Gayán, P.; García-Labiano, F.; de Diego, L. F.; Adánez, J.; Abad, A. Development of CuO-based oxygen-carrier materials suitable for chemical-looping with oxygen uncoupling (CLOU) process. *Energy Procedia* **2011**, *4*, 417−424.

(16) Adánez-Rubio, I.; Abad, A.; Gayán, P.; de Diego, L. F.; García-Labiano, F.; Adánez, J. Identification of operational regions in the chemical-looping with oxygen uncoupling (CLOU) process with a Cu-based oxygen carrier. *Fuel* **2012**, *102*, 634−645.

(17) Gayán, P.; Adánez-Rubio, I.; Abad, A.; de Diego, L. F.; García-Labiano, F.; Adánez, J. Development of Cu-based oxygen carriers for chemical-looping with oxygen uncoupling (CLOU) process. *Fuel* **2012**, *96*, 226−238.

(18) Adánez-Rubio, I.; Gayán, P.; Abad, A.; de Diego, L. F.; García-Labiano, F.; Adánez, J. Evaluation of a spray-dried $CuO/MgAl_2O_4$ oxygen carrier for the chemical looping with oxygen uncoupling process. *Energy Fuels* **2012**, *26* (5), 3069−3081.
(19) Sahir, A. H.; Sohn, H. Y.; Leion, H.; Lighty, J. S. Rate analysis of chemical-looping with oxygen uncoupling (CLOU) for solid fuels. *Energy Fuels* **2012**, *26* (7), 4395−4404.
(20) Mattisson, T.; Leion, H.; Lyngfelt, A. Chemical-looping with oxygen uncoupling using CuO/ZrO_2 with petroleum coke. *Fuel* **2009**, *88* (4), 683−690.
(21) Leion, H.; Mattisson, T.; Lyngfelt, A. Using chemical-looping with oxygen uncoupling (CLOU) for combustion of six different solid fuels. *Energy Procedia* **2009**, *1* (1), 447−453.
(22) Wen, Y.-y.; Li, Z.-s.; Xu, L.; Cai, N.-s. Experimental study of natural cu ore particles as oxygen carriers in chemical looping with oxygen uncoupling (CLOU). *Energy Fuels* **2012**, *26* (6), 3919−3927.
(23) Eyring, E. M.; Konya, G.; Lighty, J. S.; Sahir, A. H.; Sarofim, A. F.; Whitty, K. Chemical looping with copper oxide as carrier and coal as fuel. *Oil Gas Sci. Technol.* **2011**, *66* (2), 209−221.
(24) Chadda, D.; Ford, J. D.; Fahim, M. A. Chemical energy storage by the reaction cycle CuO/Cu_2O. *Int. J. Energy Res.* **1989**, *13* (1), 63−73.
(25) Arjmand, M.; Keller, M.; Leion, H.; Mattisson, T.; Lyngfelt, A. Oxygen release and oxidation rates of $MgAl_2O_4$-supported CuO oxygen carrier for chemical-looping combustion with oxygen uncoupling (CLOU). *Energy Fuels* **2012**, *26* (11), 6528−6539.
(26) Whitty, K.; Clayton, C. Measurement and modeling of kinetics for copper-based chemical looping with oxygen uncoupling. *Proceedings of the 2nd International Conference on Chemical Looping*; Darmstadt, Germany, Sept 26−28, 2012; pp 1−10.
(27) Song, H.; Shah, K.; Doroodchi, E.; Wall, T.; Moghtaderi, B. Evaluation of suitable oxygen carriers for chemical looping air separation (CLAS) for large scale oxygen production. *Proceedings of the 2nd International Conference on Chemical Looping*; Darmstadt, Germany, Sept 26−28, 2012; pp 1−9.
(28) Gayán, P.; Forero, C. R.; Abad, A.; de Diego, L. F.; García-Labiano, F.; Adánez, J. Effect of support on the behavior of Cu-based oxygen carriers during long-term CLC operation at temperatures above 1073 K. *Energy Fuels* **2011**, *25* (3), 1316−1326.
(29) Li, X.; Song, H.; Wang, Q.; Meesri, C.; Wall, T.; Yu, J. Experimental study on drying and moisture re-adsorption kinetics of an Indonesian low rank coal. *J. Environ. Sci.* **2009**, *21-S1*, S127−S130.
(30) Halikia, I.; Neou-Syngouna, P.; Kolitsa, D. Isothermal kinetic analysis of the thermal decomposition of magnesium hydroxide using thermogravimetric data. *Thermochim. Acta* **1998**, *320* (1−2), 75−88.
(31) Perkins, C.; Lichty, P.; Weimer, A. W. Determination of aerosol kinetics of thermal ZnO dissociation by thermogravimetry. *Chem. Eng. Sci.* **2007**, *62* (21), 5952−5962.
(32) Kubaschewsk, O.; Alcock, C. B. *Metallurgical Thermochemistry*, 5th ed.; Pergamon: Oxford, U.K., 1979.
(33) Pineau, A.; Kanari, N.; Gaballah, I. Kinetics of reduction of iron oxides by H_2: Part I. Low temperature reduction of hematite. *Thermochim. Acta* **2006**, *447* (1), 89−100.
(34) Pineau, A.; Kanari, N.; Gaballah, I. Kinetics of reduction of iron oxides by H_2: Part II. Low temperature reduction of magnetite. *Thermochim. Acta* **2007**, *456* (2), 75−88.
(35) Zhu, Y.; Mimura, K.; Isshiki, M. Oxidation mechanism of Cu_2O to CuO at 600−1050 °C. *Oxid. Met.* **2004**, *62* (3), 207−222.
(36) Meijering, J. L.; Verheijke, M. L. Oxidation kinetics in the case of ageing oxide films. *Acta Metall.* **1959**, *7* (5), 331−338.